JACS
JOURNAL OF THE AMERICAN CHEMICAL SOCIETY
Article
pubs.acs.org/JACS

# Efficient Electrochemical Reduction of Carbon Dioxide to Acetate on Nitrogen-Doped Nanodiamond

Yanming Liu, Shuo Chen, Xie Quan,* and Hongtao Yu

Key Laboratory of Industrial Ecology and Environmental Engineering (Ministry of Education, China), School of Environmental Science and Technology, Dalian University of Technology, Dalian 116024, China

Supporting Information

**ABSTRACT:** Electrochemical reduction of $CO_2$ is an attractive technique for reducing $CO_2$ emission and converting it into useful chemicals, but it suffers from high overpotential, low efficiency or poor product selectivity. Here, N-doped nanodiamond/Si rod array (NDD/Si RA) was proposed as an efficient nonmetallic electrocatalyst for $CO_2$ reduction. It preferentially and rapidly converted $CO_2$ to acetate over formate with an onset potential of −0.36 V (vs RHE), overcoming the usual limitation of low selectivity for C2 products. Moreover, faradic efficiency of 91.2−91.8% has been achieved for $CO_2$ reduction at −0.8 to −1.0 V. Its superior performance for $CO_2$ reduction can be attributed to its high overpotential for hydrogen evolution and N doping, where N-$sp^3$C species was highly active for $CO_2$ reduction. Electrokinetic data and *in situ* infrared spectrum revealed the main pathway for $CO_2$ reduction might be $CO_2 \rightarrow CO_2^{\bullet-} \rightarrow (COO)_2^{\bullet} \rightarrow CH_3COO^-$.

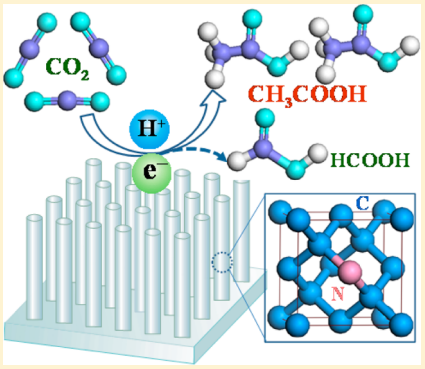


## 1. INTRODUCTION

As the main energy sources, fossil fuels have been used worldwide and led to increased emission of $CO_2$ (greenhouse gas). Converting $CO_2$ into valuable fuels or chemicals is an attractive solution to prevent $CO_2$ accumulation in atmosphere. The approaches for $CO_2$ conversion include radiochemical, thermochemical, biochemical, photochemical, and electrochemical methods.[1−4] Among them, electrochemical reduction is favored because it can be powered by a renewable electricity source, proceeds at moderate temperature and atmospheric pressure, and the products can be tuned by varying reaction conditions.[4,5] Fuel or chemical synthesis using $CO_2$, $H_2O$, and renewable energy is a simplified artificial photosynthesis, which is of great interest for the development of sustainable energy economy. Challenges for electrochemical reduction of $CO_2$ are the development of active and robust electrocatalysts, which should have high efficiency, low overpotential for selectively reducing $CO_2$ to one or two of many possible products (C1: CO, $CH_4$, $CH_3OH$, HCOOH. C2: $C_2H_4$, $C_2H_5OH$, $CH_3COOH$, etc.) while inhibiting hydrogen evolution. Converting $CO_2$ to C2 products are favorable because industrial synthesis of C2 products is usually more complicated and energy intensive than that of C1 products.

Various metal electrocatalysts (such as Au, Ag, Pt, Cu, Sn) have been extensively studied for electrochemical reduction of $CO_2$.[6−10] Unfortunately, for many polycrystalline metals, they suffered from one or more of the following problems: low efficiency due to hydrogen evolution, poor product selectivity, high overpotential, easy deactivation, and limited supply of noble metals. Recently, researches attempted to improve their performance from structure design, employing ionic liquid, metal oxides or metal chalcogenides.[11−15] Meanwhile, it has been discovered that nonmetallic electrocatalysts based on carbon were also active for electrochemical reduction.[16−18] Only a few carbon electrocatalysts have been reported for $CO_2$ reduction, including B-doped diamond, N-doped graphitic carbon and cobalt complex modified diamond.[18−21] Notably, these electrocatalysts all convert $CO_2$ to C1 products. Despite the progress, it is still desirable to develop robust carbon electrocatalysts with low overpotential, high efficiency and fast kinetics for $CO_2$ reduction, especially converting $CO_2$ to C2 products.

N-doped nanodiamond is advantageous over metal and other semiconductors for electrocatalysis due to its interesting properties. Its overpotential for hydrogen evolution is higher than most reported electrocatalysts,[22] including metals, B-doped diamond and graphitic carbon materials. During the process of $CO_2$ reduction, large overpotential will inhibit $H_2O$ reduction and results in high energy efficiency and fast kinetics for electrochemical reduction of $CO_2$. Besides, N-doped nanodiamond has excellent chemical stability even in harsh media,[23] which keeps it highly active for $CO_2$ reduction in a long-term operation. Moreover, strain and defect sites induced by N-doping can provide active sites for electrochemical reaction.[24] The positively charged carbon atoms from N polarization may facilitate the adsorption of $CO_2$ and $CO_2^{\bullet-}$, inducing a reduced energy barrier toward electrochemical reactions. However, to date N-doped diamond has not been explored for electrocatalytic $CO_2$ reduction as well as the correlation between N species and $CO_2$ reduction activity. Here, N-doped nanodiamond/Si rod array (NDD/Si RA)

Received: March 22, 2015
Published: August 31, 2015





DOI: 10.1021/jacs.5b02975
J. Am. Chem. Soc. 2015, 137, 11631−11636

electrode was proposed for electrochemical reduction of $CO_2$, which showed high efficiency, fast kinetics, and good selectivity for converting $CO_2$ to acetate. The relationship between N types and $CO_2$ reduction activity was investigated. Electrokinetic data and *in situ* infrared spectrum were employed to analyze the mechanism for electrochemical reduction of $CO_2$ on NDD/Si RA electrode.

## 2. RESULTS AND DISCUSSION

**2.1. Preparation and Characterization of NDD/Si RA.** The typical process for NDD/Si RA preparation is shown in Scheme 1. Briefly, the Si (resistivity of 0.001 Ω·cm) RA substrate was fabricated by photolithography (details have been described in our previous work[22]). To increase nucleation density during NDD film deposition, Si RA substrate was ultrasonically treated in a nanodiamond suspension. Subsequently, NDD film was deposited on the pretreated substrate by microwave plasma enhanced chemical vapor deposition (the reason for using Si as substrate was illustrated in Supporting Information). The deposition conditions were as follows: $N_2$(1.5%)/$CH_4$(1.0%)/$H_2$ (97.5%), pressure 5.6−6.0 kPa, temperature 450 or 500 °C, time 10 h. The NDD/Si RAs prepared at 450 and 500 °C were denoted as $NDD_L$/Si RA and $NDD_H$/Si RA, respectively.

**Scheme 1. Schematic Illustration of the Process for NDD/Si RA Preparation**

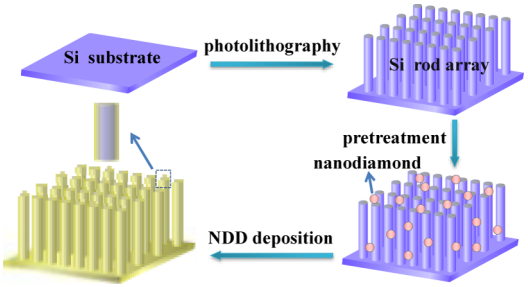


The SEM images (Figure 1) show the morphology of synthesized $NDD_L$/Si RA and $NDD_H$/Si RA, which are vertically aligned rod arrays with NDD/Si rod height about 20.0 μm. NDD films cover the entire substrates without any noticeable crack, as revealed by the different morphologies between NDD/Si RAs and Si RA substrate (Figure S1). High-resolution SEM images show the NDD films are composed of NDD nanoparticles and the nanoparticle size of $NDD_L$/Si RA is similar to that of $NDD_H$/Si RA, which is in the range of 30−120 nm. Two diffraction peaks at 43.9° and 75.3°, corresponding to (111) and (220) planes of cubic diamond (JCPDS no. 06-0675), are observed in the XRD spectra of both $NDD_L$/Si RA and $NDD_H$/Si RA (Figure S2). These results demonstrate that $NDD_L$/Si RA and $NDD_H$/Si RA have similar morphology and the same crystal structure.

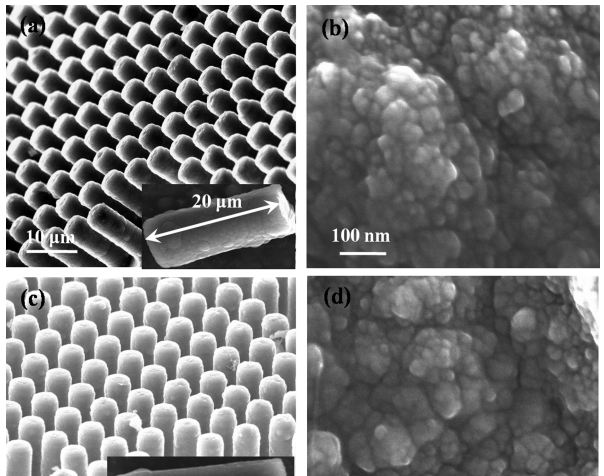


**Figure 1.** SEM images of (a and b) $NDD_L$/Si RA and (c and d) $NDD_H$/Si RA.

**2.2. Electrochemical Reduction of $CO_2$.** To evaluate the electrochemical behavior of $NDD_L$/Si RA and $NDD_H$/Si RA electrodes for $CO_2$ reduction, linear sweep voltammetry test was first performed in $CO_2$ or Ar saturated 0.5 M $NaHCO_3$ solution. As shown in Figure 2, obvious reduction peaks are observed for both $NDD_L$/Si RA and $NDD_H$/Si RA electrodes under $CO_2$ atmosphere, whereas no reduction peak appears at their linear sweep voltammograms under Ar atmosphere (with the absence of $CO_2$), demonstrating that $CO_2$ can be electrochemically reduced on both $NDD_L$/Si RA and $NDD_H$/Si RA electrodes. The onset potential for $CO_2$ reduction is −0.36 V (vs RHE) on $NDD_L$/Si RA electrode, much more positive than that of $NDD_H$/Si RA electrode (−0.60 V). It should be noted that the onset potential for $CO_2$ reduction on $NDD_L$/Si RA electrode is also more positive than most of nonprecious electrocatalysts reported recently.[5,14,21]

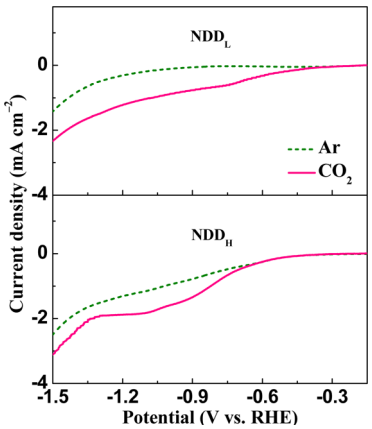


**Figure 2.** Linear sweep voltammograms of $NDD_L$/Si RA and $NDD_H$/Si RA electrodes in Ar (dashed line) or $CO_2$ (solid line) saturated 0.5 M $NaHCO_3$ solution (scan rate of 50 mV $s^{-1}$).

The performance of NDD/Si RA electrodes for electrocatalytic $CO_2$ reduction was further examined by conducting constant-potential electrolysis in $CO_2$ saturated $NaHCO_3$ solution. The applied potential for electrolysis was selected in the range of −0.55 to −1.30 V based on the onset potential for $CO_2$ reduction and hydrogen evolution on NDD/Si RA electrodes (Figure 2). During the process of $CO_2$ reduction, the main products detected were acetate and formate for both $NDD_L$/Si RA and $NDD_H$/Si RA electrodes (the Si substrate was proved to be inert for electrocatalytic $CO_2$ reduction based on the result of $CO_2$ electrolysis and cyclic voltammograms of Figure S3). Figure 3 presents their average production rates for acetate and formate under various potentials, which are obtained from the data of electrochemical reduction of $CO_2$


DOI: 10.1021/jacs.5b02975
J. Am. Chem. Soc. 2015, 137, 11631−11636

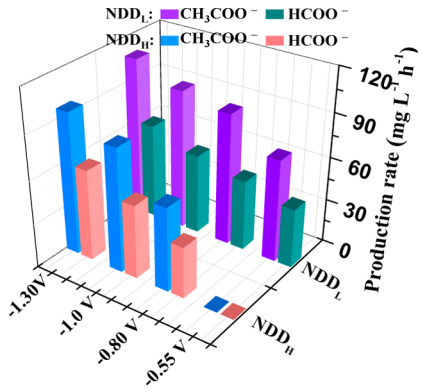


**Figure 3.** Production rates of acetate and formate on NDD$_L$/Si RA and NDD$_H$/Si RA electrodes obtained from electrochemical reduction of $CO_2$ for 3 h at −0.55 to −1.30 V ($CO_2$ saturated 0.5 M $NaHCO_3$).

for 3 h. Interestingly, NDD$_L$/Si RA and NDD$_H$/Si RA electrodes can preferentially convert $CO_2$ to acetate under any applied potential that $CO_2$ can be reduced in this experiment. The production rate of acetate is 1.65−1.90 times as great as that of formate for NDD$_L$/Si RA electrode at −0.55 to −1.30 V, while it is 1.55−1.67 times as great as that of formate for NDD$_H$/Si RA electrode under the same conditions. Both production rates of acetate and formate increase when the potential is negatively shifted from −0.55 to −1.30 V. Under the same potential, NDD$_L$/Si RA electrode presents larger production rates for acetate and formate relative to NDD$_H$/Si RA electrode, suggesting its much faster $CO_2$ conversion rate. High production rates of acetate have been achieved on NDD$_L$/Si RA electrode, which are 96.1 mg L$^{-1}$ h$^{-1}$ at −1.0 V. These results suggest the performance of NDD$_L$/Si RA electrode for electrochemical $CO_2$ reduction is superior to that of NDD$_H$/Si RA electrode. To verify acetate and formate derived from $CO_2$ reduction, electrolysis experiment was performed on NDD$_L$/Si RA electrode in $N_2$ saturated $NaHCO_3$ solution (without $CO_2$) at −1.0 V. Acetate and formate were undetectable after electrolysis for 2 h, confirming acetate and formate were derived from $CO_2$ reduction rather than $HCO_3^-$ reduction.

It has been reported that the type of N species and N-doping level correlate to electrocatalytic activity of N-doped carbon materials during oxygen reduction and water splitting.[24,25] To gather insight into the much higher activity of NDD$_L$/Si RA electrode for $CO_2$ reduction, its N content and the type of N species were determined by XPS spectrum (Figure 4). The N content is 2.12 atom % for NDD$_L$/Si RA electrode, similar to

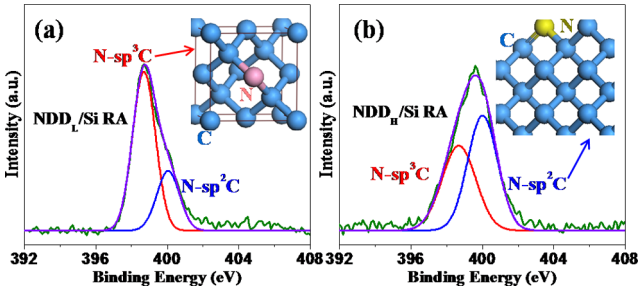


**Figure 4.** N 1s XPS spectra of (a) NDD$_L$/Si RA and (b) NDD$_H$/Si RA electrodes. The inset shows chemical structure of NDD with (a) N-sp$^3$C and (b) N-sp$^2$C species.

that of NDD$_H$/Si RA electrode (2.30 atom %). Although peaks associated with N-sp$^3$C (398.7 eV) and N-sp$^2$C (400.1 eV) are observed on both electrodes, N species of NDD$_L$/Si RA is dominated by N-sp$^3$C, while the main N species of NDD$_H$/Si RA is N-sp$^2$C. Since NDD$_L$/Si RA and NDD$_H$/Si RA electrodes have the same crystal structure, similar morphology and N content, it can be deduced that N-sp$^3$C is more active than N-sp$^2$C for electrocatalytic reduction of $CO_2$. Meanwhile, in order to understand the influence of N content on $CO_2$ reduction activity, NDD$_L$/Si RA electrodes with N contents of 0.93 and 3.68 atom % were prepared at 450 °C and their performance for $CO_2$ reduction was investigated at −1.0 V. As displayed in Figure 5, the production rates for acetate and

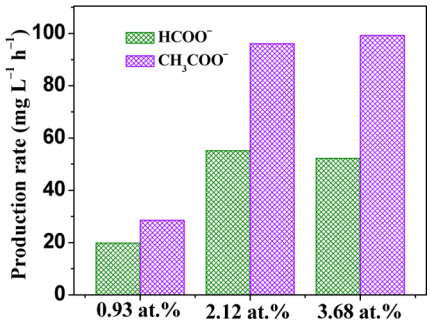


**Figure 5.** Production rates of acetate and formate on NDD$_L$/Si RA electrodes with N contents of 0.93, 2.12, and 3.68 atom % (−1.0 V).

formate are significantly enhanced as the N content increases from 0.93 to 2.12 atom %, indicating increase of N content promotes $CO_2$ conversion. However, the enhancement is not obvious when N content is further increased to 3.68 atom %. N 1s XPS spectra reveal that the N specie is also dominated by N-sp$^3$C for NDD$_L$/Si RA electrodes with N contents of 0.93 and 3.68 atom % (Figure S4). When N content increases from 2.12 to 3.68 atom %, the almost unchanged production rate may be attributed to the positively shifted hydrogen evolution potential (Figure S5).

Energy efficiency is one of the major concerns for electrocatalysis. Achieving high energy efficiency remains a great challenge for electrocatalytic reduction of $CO_2$. Here, faradic efficiency for electrochemical reduction of $CO_2$ was investigated on NDD$_L$/Si RA electrode (its current−time curves for $CO_2$ electrolysis were presented in Figure S6). Figure 6 illustrates its faradic efficiency for generating acetate and formate at various potentials. As expected, the faradic efficiency

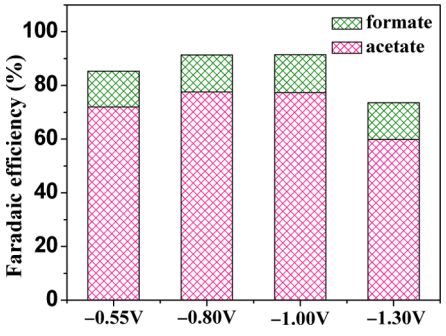


**Figure 6.** Faradaic efficiency for acetate and formate production for electrochemical reduction of $CO_2$ on NDD$_L$/Si RA electrode at −0.55 to −1.30 V ($CO_2$ saturated 0.5 M $NaHCO_3$ solution).



DOI: 10.1021/jacs.5b02975
J. Am. Chem. Soc. 2015, 137, 11631−11636

for acetate production is significantly higher than that for formate production at any potential applied (−0.55 to −1.3 V). At −0.8 to approximately −1.0 V, the faradic efficiency is about 77.3−77.6% for acetate production and 13.6−14.6% for formate production. The total faradic efficiency increases initially (−0.55 to −1.0 V) and then declines as the potential is negatively shifted, reaching the maximum of 91.8% at −1.0 V. It is worth noting that the total faradic efficiency of $NDD_L$/Si RA electrode is comparable to or even much higher than those of $SnO_2$, Au, boron doped diamond,[9,14,18] which are among the best electrocatalysts for $CO_2$ reduction reported recently. The faradic efficiency decline at −1.30 V may be attributed to hydrogen generation, which can be verified from the hydrogen evolution potential (about −1.10 V vs RHE) in Figure 2.

The stability of $NDD_L$/Si RA electrode for electrochemical reduction of $CO_2$ was evaluated by 10 successive batches of $CO_2$ electrolysis at −1.0 V (each batch lasted 3 h). As shown in Figure S7, the production rates remain around 96.1 mg $L^{-1}$ $h^{-1}$ for acetate and 55.2 mg $L^{-1}$ $h^{-1}$ for formate during 10 successive batches, indicating no deactivation occurs on $NDD_L$/Si RA electrode. These results verify the good stability of $NDD_L$/Si RA electrode for electrochemical reduction of $CO_2$.

**2.3. Discussion.** Electrokinetic data were determined to probe the mechanism of $CO_2$ reduction. Figure 7a shows the

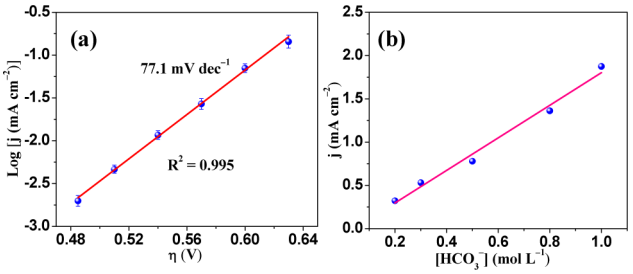


**Figure 7.** (a) Tafel plot for acetate production; (b) current density for $CO_2$ reduction versus $NaHCO_3$ concentration at −1.0 V.

plot of overpotential versus partial current density for acetate production on $NDD_L$/Si RA electrode (Tafel plot). This plot presents good linearity with a slope of 77.1 mV $dec^{-1}$. Possibilities for the chemical rate-determining step of $CO_2$ reduction include single-electron transfer to $CO_2$ (Tafel slope about 118 mV $dec^{-1}$) and single-electron transfer to $CO_2$ prior to a chemical rate-determining step (Tafel slope about 59 mV $dec^{-1}$).[11,14,26] The Tafel slope of 77.1 mV $dec^{-1}$ suggests single-electron transfer to $CO_2$ is not the rate-determining step for $CO_2$ reduction. The higher acetate production rate (relative to formate) on $NDD_L$/Si RA electrode indicates that C−C coupling is fast once $CO_2$ reduction initiates. To probe the influence of $HCO_3^-$ concentration, electrocatalytic $CO_2$ reduction was carried out at $NaHCO_3$ electrolyte with concentrations ranging from 0.2 to 1.0 mol $L^{-1}$ ($NaClO_4$ was added to the electrolyte to maintain the conductivity). The current density for $CO_2$ reduction increases linearly with the concentration of $HCO_3^-$ (Figure 7b), indicating dependence of $CO_2$ reduction rate on $HCO_3^-$ concentration. This phenomenon can be attributed to proton transfer from $HCO_3^-$ (proton from $HCO_3^-$ rather than $H_2O$ was explained in Supporting Information) during $CO_2$ reduction on $NDD_L$/Si RA electrode.

The pathway for electrochemical reduction of $CO_2$ on $NDD_L$/Si RA electrode was studied by *in situ* infrared spectrum with external reflection mode. Figure 8 shows the electrolysis time-dependent infrared spectrum for electrocatalytic $CO_2$

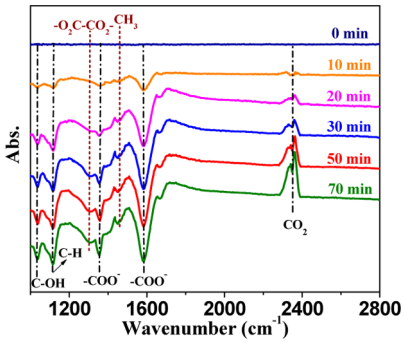


**Figure 8.** *In situ* infrared spectrum of $CO_2$ reduction on $NDD_L$/Si RA electrode at −1.0 V with different electrolysis time ($CO_2$ saturated 0.5 mol $L^{-1}$ $NaHCO_3$ solution).

reduction on NDDL/Si RA electrode at −1.0 V, where the signal of $CO_2$ saturated $NaHCO_3$ solution was used as the background. No peak can be observed from the infrared spectrum until electrolysis started. The upward band at 2431 and 2462 $cm^{-1}$ is associated with $CO_2$. Its intensity increases as the electrolysis time increases, illustrating the gradual consumption of $CO_2$. The peak at 1307 $cm^{-1}$ is attributed to OOC−COO.[27] Its intensity also increases initially during the first 30 min and then almost remains unchanged for further electrolysis, suggesting OOC−COO may be the intermediate of $CO_2$ reduction. The band related to C−H of $CH_3$ is detected at 1450 $cm^{-1}$. The formation of $COO^-$ can be verified from the peaks at 1352 and 1580 $cm^{-1}$ (bridge-bonded and dissolved form).[28] In addition, the peaks related to C−H and C−OH are observed at 1116 and 1036 $cm^{-1}$, respectively.

On the basis of the results of infrared spectrum and products detected, along with mechanism reported,[5] the possible pathway for electrochemical reduction of $CO_2$ on $NDD_L$/Si RA electrode is proposed as follows (Figure 9). First, $CO_2$ is

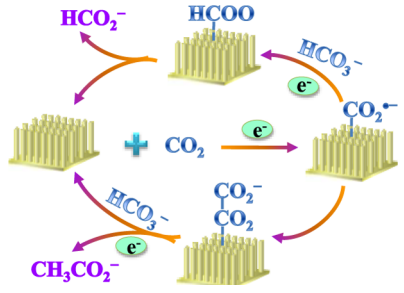


**Figure 9.** Schematic pathway for electrocatalytic $CO_2$ reduction on $NDD_L$/Si RA electrode.

adsorbed on the electrode surface and reduced to $CO_2^{\bullet-}$. Subsequently, (1) the $CO_2^{\bullet-}$ radical is protonated by the proton from $HCO_3^-$ and electrochemically reduced to $(HCOO)_{abs}$, leading to the formation of formate; (2) since the kinetics for $CO_2^{\bullet-}$ formation is fast (based on the mechanism that single-electron transfer to $CO_2$ to generate $CO_2^{\bullet-}$ prior to a chemical rate-determining step), the formed $CO_2^{\bullet-}$ radical can combine with another one and generate OOC−COO. The OOC−COO is then protonated and further reduced, resulting in the production of acetate (this pathway is


DOI: 10.1021/jacs.5b02975
J. Am. Chem. Soc. 2015, 137, 11631−11636

also supported by the result of oxalate reduction at $NDD_L$/Si RA electrode, which shows acetate is the reduction product of oxalate, details in Supporting Information). Here, the production rate of acetate is greater than that of formate, which may be due to that the kinetics for $CO_2 \rightarrow CO_2^{\bullet-}$ and/or C−C coupling is faster than $CO_2^{\bullet-}$ protonation.[26] It has been reported that $CO_2$ was reduced to C1 products on N-doped graphitc carbon (HCOOH, CO) or B-doped diamond electrodes (HCHO).[18,19,21] It can be deduced that N-doping or $sp^3$-C individual may be not responsible for the high acetate selectivity of NDD/Si RA electrode. The high acetate selectivity of NDD/Si RA electrode is probably correlated to the intrinsic property of NDD. Further studies are required to understand the origin of acetate selectivity.

The high electrocatalytic activity of $NDD_L$/Si RA electrode can be attributed to several factors. As evident from the electrocatalytic activity of $NDD_L$/Si RA with different N contents, a fine balance between N content and hydrogen evolution potential is essential for achieving high performance for electrochemical $CO_2$ reduction. Some recent studies for related carbon materials show N-doping can induce defect sites and the doped N atoms can polarize the adjacent carbon atoms.[29,30] The resulted positively charged carbon atoms and defects may promote $CO_2$ adsorption onto the catalytic surfaces and stabilize the produced $CO_2^{\bullet-}$ through electronic interaction, thereby reducing the energy barrier and facilitating $CO_2$ reduction. Moreover, $NDD_L$/Si RA electrode has a high overpotential for hydrogen evolution, inhibiting $H_2O$ reduction and improving the efficiency for $CO_2$ reduction. According to the results of $CO_2$ reduction on $NDD_L$/Si RA and $NDD_H$/Si RA electrodes, N-$sp^3$C is more efficient than N-$sp^2$C for electrochemical reduction of $CO_2$. The high N-$sp^3$C content of $NDD_L$/Si RA electrode also contributes to its good activity. Besides, the vertically aligned rod array structure allows large area of electrode surface to interact with reactants and provides direct channels for efficient electron transport during electrocatalytic $CO_2$ reduction. Therefore, the high electrocatalytic activity of $NDD_L$/Si RA electrode for $CO_2$ reduction is most likely originated from its high N content (doping related defect sites and charge polarization), high overpotential for hydrogen evolution, and large fraction of N-$sp^3$C, as well as fast electron transfer.

## 3. CONCLUSION

In summary, NDD/Si RA, consisting of earth abundant components, is an efficient and stable nonmetallic material for electrocatalytic $CO_2$ reduction. It converted $CO_2$ to acetate and formate with fast kinetics, where production rate of acetate was 1.65−1.90 times as great as that of formate. Meanwhile, NDD/Si RA presented notable current efficiency (91.2−91.8% at −0.8 to −1.0 V) and longevity for electrocatalytic $CO_2$ reduction. The superior performance of NDD/Si RA resulted from its high hydrogen evolution potential and N-doping, where N-$sp^3$C was the most active species. Electrokinetic data and *in situ* infrared spectrum revealed the pathway for $CO_2$ reduction on NDD/Si RA might be $CO_2 \rightarrow CO_2^{\bullet-} \rightarrow (COO)_2^{\bullet} \rightarrow CH_3COO^-$. This work opens up a new avenue for the development of carbon-based electrocatalytic material for $CO_2$ reduction and converting $CO_2$ to C2 products.

## ■ ASSOCIATED CONTENT

### Supporting Information

The Supporting Information is available free of charge on the ACS Publications website at DOI: 10.1021/jacs.5b02975.

Experimental details; characterization data (PDF)

## ■ AUTHOR INFORMATION


### Corresponding Author

*quanxie@dlut.edu.cn


### Notes

The authors declare no competing financial interest.

## ■ ACKNOWLEDGMENTS

This work was supported by National Basic Research Program of China (2011CB936002), National Natural Science Foundation of China (NO.21437001) and PCSIRT_13R05.

## ■ REFERENCES


(1) Kondratenko, E. V.; Mul, G.; Baltrusaitis, J.; Larrazábal, G. O.; Pérez-Ramírez, J. *Energy Environ. Sci.* **2013**, *6*, 3112.
(2) Mikkelsen, M.; Jørgensen, M.; Krebs, F. C. *Energy Environ. Sci.* **2010**, *3*, 43.
(3) Qiao, J.; Liu, Y.; Hong, F.; Zhang, J. *Chem. Soc. Rev.* **2014**, *43*, 631.
(4) Costentin, C.; Robert, M.; Saveant, J. M. *Chem. Soc. Rev.* **2013**, *42*, 2423.
(5) Kuhl, K. P.; Cave, E. R.; Abram, D. N.; Jaramillo, T. F. *Energy Environ. Sci.* **2012**, *5*, 7050.
(6) Centi, G.; Perathoner, S.; Win, G.; Gangeri, M. *Green Chem.* **2007**, *9*, 671.
(7) Lu, Q.; Rosen, J.; Zhou, Y.; Hutchings, G. S.; Kimmel, Y. C.; Chen, J. G.; Jiao, F. *Nat. Commun.* **2014**, *5*, 3242.
(8) Nie, X.; Esopi, M. R.; Janik, M. J.; Asthagiri, A. *Angew. Chem., Int. Ed.* **2013**, *52*, 2459.
(9) Zhu, W.; Michalsky, R.; Metin, O.; Lv, H.; Guo, S.; Wright, C. J.; Sun, X.; Peterson, A. A.; Sun, S. *J. Am. Chem. Soc.* **2013**, *135*, 16833.
(10) Hori, Y.; Wakebe, H.; Tsukamoto, T.; Koga, O. *Electrochim. Acta* **1994**, *39*, 1833.
(11) Chen, Y.; Li, C. W.; Kanan, M. W. *J. Am. Chem. Soc.* **2012**, *134*, 19969.
(12) Lim, H. K.; Shin, H.; Goddard, W. A.; Hwang, Y. J.; Min, B. K.; Kim, H. *J. Am. Chem. Soc.* **2014**, *136*, 11355.
(13) Rosen, B. A.; Salehi-Khojin, A.; Thorson, M. R.; Zhu, W.; Whipple, D. T.; Kenis, P. J.; Masel, R. I. *Science* **2011**, *334*, 643.
(14) Zhang, S.; Kang, P.; Meyer, T. J. *J. Am. Chem. Soc.* **2014**, *136*, 1734.
(15) Asadi, M.; Kumar, B.; Behranginia, A.; Rosen, B. A.; Baskin, A.; Repnin, N.; Pisasale, D.; Phillips, P.; Zhu, W.; Haasch, R.; Klie, R. F.; Kral, P.; Abiade, J.; Salehi-Khojin, A. *Nat. Commun.* **2014**, *5*, 4470.
(16) Zheng, Y.; Jiao, Y.; Jaroniec, M.; Qiao, S. Z. *Angew. Chem., Int. Ed.* **2015**, *54*, 52.
(17) Zheng, Y.; Jiao, Y.; Zhu, Y.; Li, L. H.; Han, Y.; Chen, Y.; Du, A.; Jaroniec, M.; Qiao, S. Z. *Nat. Commun.* **2014**, *5*, 3783.
(18) Kumar, B.; Asadi, M.; Pisasale, D.; Sinha-Ray, S.; Rosen, B. A.; Haasch, R.; Abiade, J.; Yarin, A. L.; Salehi-Khojin, A. *Nat. Commun.* **2013**, *4*, 2819.
(19) Nakata, K.; Ozaki, T.; Terashima, C.; Fujishima, A.; Einaga, Y. *Angew. Chem., Int. Ed.* **2014**, *53*, 871.
(20) Yao, S. A.; Ruther, R. E.; Zhang, L.; Franking, R. A.; Hamers, R. J.; Berry, J. F. *J. Am. Chem. Soc.* **2012**, *134*, 15632.
(21) Zhang, S.; Kang, P.; Ubnoske, S.; Brennaman, M. K.; Song, N.; House, R. L.; Glass, J. T.; Meyer, T. J. *J. Am. Chem. Soc.* **2014**, *136*, 7845.
(22) Liu, Y. M.; Chen, S.; Quan, X.; Fan, X. F.; Zhao, H. M.; Zhao, Q.; Yu, H. T. *Appl. Catal., B* **2014**, *154−155*, 206.




DOI: 10.1021/jacs.5b02975
*J. Am. Chem. Soc.* 2015, 137, 11631−11636

(23) Mochalin, V. N.; Shenderova, O.; Ho, D.; Gogotsi, Y. *Nat. Nanotechnol.* **2012**, *7*, 11.
(24) Zheng, Y.; Jiao, Y.; Li, H.; Xing, T.; Chen, Y.; Jaroniec, M.; Qiao, S. Z. *ACS Nano* **2014**, *8*, 5290.
(25) Kong, X. K.; Chen, C. L.; Chen, Q. W. *Chem. Soc. Rev.* **2014**, *43*, 2841.
(26) Li, C. W.; Ciston, J.; Kanan, M. W. *Nature* **2014**, *508*, 504.
(27) Muthusamy, M.; Burrell, M. R.; Thorneley, R. N. F.; Bornemann, S. *Biochemistry* **2006**, *45*, 10667.
(28) Yang, Y. Y.; Ren, J.; Zhang, H. X.; Zhou, Z. Y.; Sun, S. G.; Cai, W. B. *Langmuir* **2013**, *29*, 1709.
(29) Liu, Y. M.; Yu, H. T.; Quan, X.; Chen, S.; Zhao, H. M.; Zhang, Y. B. *Sci. Rep.* **2014**, *4*, 6843.
(30) Wang, D. W.; Su, D. S. *Energy Environ. Sci.* **2014**, *7*, 576.



DOI: 10.1021/jacs.5b02975
*J. Am. Chem. Soc.* 2015, 137, 11631−11636